ChemComm

COMMUNICATION

View Article Online
View Journal | View Issue

Cite this: *Chem. Commun.*, 2018, 54, 6177

Received 7th May 2018,
Accepted 22nd May 2018

DOI: 10.1039/c8cc03672a

rsc.li/chemcomm

Highly-efficient and low-temperature perovskite solar cells by employing a Bi-hole transport layer consisting of vanadium oxide and copper phthalocyanine†

Ting Lei,[a] Hua Dong,*[a] Jun Xi,[ab] Yong Niu,[a] Jie Xu,[a] Fang Yuan,[a] Bo Jiao,[a] Wenwen Zhang,[c] Xun Hou[a] and Zhaoxin Wu*[ad]

In this article, an inorganic–organic bilayer hole transport layer (B-HTL) is designed and utilized in planar perovskite solar cells. Here the B-HTL consists of an inorganic VO_x matrix and a copper phthalocyanine (CuPc) buffer layer, providing excellent resistance to moisture as well as the alignment of the interfacial energy level. Benefiting from this typical HTL, an enlarged built-in potential and charge extraction can be achieved in PSCs simultaneously. Correspondingly, a champion device with a B-HTL shows a 16.85% efficiency with negligible hysteresis, which is superior to that of a PSC based on a PEDOT:PSS HTL. Meanwhile, significantly prolonged stability of the PSC with the B-HTL can be observed, exhibiting only a 10% efficiency loss after 350 hours in ambient air. Moreover, such an entirely low-temperature (≤60 °C) fabrication process of this typical PSC exhibits its successful application in flexible devices.

Recently, organometal trihalide perovskite materials have attracted much attention due to their special properties, including excellent light harvesting, high carrier mobility, long carrier lifetimes, and long carrier diffusion lengths.[1] The power conversion efficiencies (PCEs) of perovskite solar cells (PSCs) have increased rapidly from 3.8% (by Miyasaka *et al.*) in 2009 to 22.1% in eight years.[2,3] In spite of the great progress in PSCs recently, the efficiency limitation and the stability of the devices are still bottlenecks, which restrict their further application in commercial areas. Among the various types of PSCs, a planar heterojunction P–I–N device is one of the most universal structures owing to the low-temperature and easy-fabrication process, where PEDOT:PSS is commonly used as the hole transport layer (HTL).[4] However, such an organic film is hydrophilic and acidic, leading to the invasion of the moisture and the degradation of the perovskite layer.[5,6] Moreover, the lower work function of PEDOT (~4.8 eV) would lead to an energy loss of charge extraction at the perovskite/HTL interface, inducing a decrease of the open-circuit voltage.[7] To overcome these shortages, hydrophobic organic materials or stable inorganic p-type materials with high work functions are developed as alternatives to PEDOT.[7–13] Among them, inorganic metal oxides can achieve both high open voltages and stability of PSCs when employed as HTLs. However, sol–gel NiO_x films require high temperature for sufficient hydrolysis and crystallization, while NiO_x nanoparticles are complexly synthesized and the coverage on the substrate is unsatisfactory.[5,14] Vanadium pentoxide (VO_x) is another alternative HTL due to its high transparency and high carrier mobility. However, there is still relative lack of attention and the reported performance of PSCs with VO_x is still limited.[15]

Therefore, to achieve a win–win situation in terms of both the outstanding performance of the PSCs and the simplicity of the fabrication process, an inorganic–organic bilayer hole transport layer (B-HTL) is designed and utilized in planar perovskite solar cells, composed of a VO_x body layer and a copper phthalocyanine (CuPc) buffer layer. The conductive VO_x film is prepared *via* a simple sol–gel method, which only requires room temperature for hydrolysis. P-type CuPc (shown in Fig. S1, ESI†) further modifies the band alignment at the HTL/perovskite interface, guaranteeing effective charge extraction. With the advantages of excellent conductive and appropriate band alignment of the B-HTL, the related PSC shows the best PCE of 16.85%, exhibiting a nearly 20% higher PCE than that of a PSC with PEDOT (14.31%). Besides their electrical properties, the inorganic VO_x matrix and hydrophobic CuPc significantly improve the stability of the device, showing a 10% efficiency loss after 350 hours in the atmosphere. Moreover, since the overall preparation processes of the PSCs are carried out under a rather low temperature (≤60 °C), a flexible device based on a B-HTL is also exploited in our experiment and shows a considerable efficiency of 14.39%.

[a] *Key Laboratory of Photonics Technology for Information, Key Laboratory for Physical Electronics and Devices of the Ministry of Education, School of Electronic and Information Engineering, Xi'an Jiaotong University, Xi'an 710049, P. R. China. E-mail: zhaoxinwu@mail.xjtu.edu.cn, donghuaxjtu@mail.xjtu.edu.cn*
[b] *Global Frontier Center for Multiscale Energy Systems, Seoul National University, Seoul 08826, Korea*
[c] *School of Electronic Engineering, Xi'an University of Posts & Telecommunications, Xi'an 710121, China*
[d] *Collaborative Innovation Center of Extreme Optics, Shanxi University, Taiyuan 030006, China*

† Electronic supplementary information (ESI) available. See DOI: 10.1039/c8cc03672a

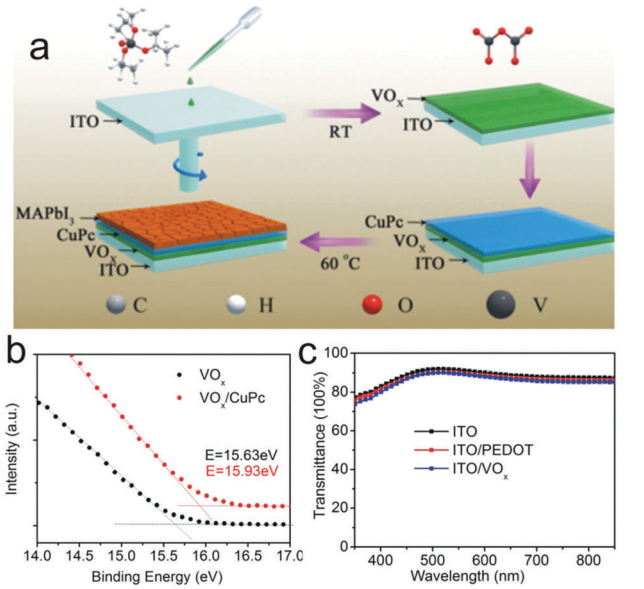

Fig. 1 (a) Schematic diagram of the B-HTL fabrication process. (b) Ultraviolet photoelectron spectroscopy of VO_x and VO_x/CuPc. (c) Transmittance spectra of different films.

A schematic representation of the B-HTL fabrication process is shown in Fig. 1a. An inorganic VO_x film is prepared by a sol–gel method, and CuPc buffer is deposited *via* an evaporation method. Fig. S2b and c (ESI†) show the top-view SEM images of the ITO/VO_x and ITO/VO_x/CuPc structures. Compared to the bare ITO (shown in Fig. S2a, ESI†), it can be seen that a continuous VO_x film covered on the ITO substrate with a uniform morphology. The transmittance spectra of the VO_x and PEDOT on the ITO substrates are also measured and are shown in Fig. 1c; both the materials exhibit a high transmittance over the visible region, which could promote the sufficient light-capturing of the PSCs.

To investigate the interfacial injection barrier at the HTL/perovskite interface, ultraviolet photoelectron spectroscopic (UPS) analysis and surface Kelvin probe (SKP) measurements are introduced to explore the work functions (W_F) of different materials. The result shows that the W_F of the as-prepared VO_x is 5.58 eV (shown in Fig. 1b and Fig. S3, ESI†), more negative than that reported for PEDOT (with the W_F of 4.8 eV). As for the planar p–i–n heterojunction device, the W_F of the HTL could affect the quasi-Fermi energy splitting of a p–n junction, thereby favoring the improvement of the open voltage.[7] However, considering that the valence band level (VB) of the $MAPbI_3$ perovskite is about 5.4 eV, imperfect band alignment still exists at the VO_x/perovskite interface.

To further tune the band alignment, a thin p-type CuPc film is introduced as the buffer layer deposited on the VO_x film. As a typical metal complex, the CuPc film has been successfully used in organic solar cells due to its high mobility and stability.[13,16–20] In addition to this, UPS and SKP measurements indicate that the surface W_F of the CuPc/VO_x structure is 5.28 eV, which is a better fit for the valence band of the $MAPbI_3$ perovskite (~5.4 eV). Hence the B-HTL is anticipated to eliminate the interfacial barrier and promote the charge extractions.

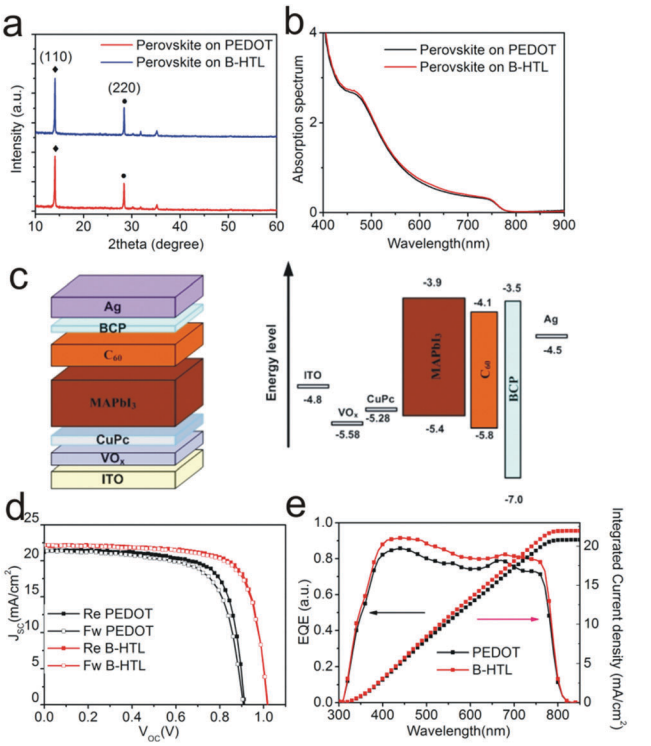

Fig. 2 (a) XRD patterns and (b) absorption spectra of $MAPHbI_3$ on different HTLs. (c) Energy diagrams of the p–i–n device. (d) *J*–*V* curves and (e) EQE and integrated J_{sc} curves of the best PSCs with different HTLs.

In our study, the fabrication approach of the perovskite is a sequential vaporing/spin-coating process. Fig. S4 (ESI†) shows the SEM images of the perovskite films on PEDOT and a B-HTL, in which both the sizes and the morphologies are very similar. X-ray diffraction analysis of the perovskite films is also carried out, and the patterns are shown in Fig. 2a. In the XRD patterns, strong diffraction peaks at 14.09° and 28.10° can be assigned to the (110) and (220) planes of the $MAPbI_3$ perovskite respectively.[21] Similar diffraction intensities of the perovskite films on different HTLs can be observed, indicating that the surface properties of the HTLs have little effect on the crystallinity of vapor-solution perovskite films. The UV-visible absorption spectra of the perovskites on the B-HTL and PEDOT are also measured and shown in Fig. 2b, and there is also no distinctly different absorption edge.

The introduction of the CuPc buffer layer is crucially important for interfacial energy level matching; meanwhile, the light-capturing behavior of the CuPc layer should also be considered seriously. Too thick a CuPc film would lead to absorption competition between the perovskite layer and the HTL, accompanied by an increased series resistance of the whole device. While a thinner buffer layer may not form a continuous coverage on the VO_x sublayer, which could be adverse to the interfacial charge collection. To determine the optimal thickness of the CuPc layer, a series of CuPc films (thicknesses = 0, 2, 5, 10, 20 nm) is exploited in our study. Fig. S5 (ESI†) shows the corresponding transmittances of the B-HTLs. As expected, the transmittance of the B-HTL decreased as the thickness of CuPC increased, which would lead to less light harvested into the perovskite layer.

In order to explore the influence of the HTL on the performance of solar cells, P–I–N planar solar cells based on different HTLs are fabricated and the energy diagrams of the p–i–n device are shown in Fig. 2c. Fig. S6 and Table S1 (ESI†) show the typical *J*–*V* curves of the PSCs with B-HTLs under 1 sun illumination. The PSCs with single-layer VO_x as the HTL show a low PCE of 11.86% with low V_{oc} and J_{sc}. This unsatisfactory performance may be attributed to the energy band split at the VO_x/perovskite interface. Interestingly, with the incorporation of the CuPc layer, the efficiencies of the PSCs are improved obviously and exhibit an increase-to-decrease tendency accompanied by an increase of the CuPc thickness, and the highest efficiency (15.98%) is achieved at 10 nm CuPc. The evolution of the device performance is according to our speculation, that is, the balance between the light-harvesting and charge extraction. We also compared the PSCs with PEDOT and an optimal B-HTL, and the *J*–*V* curves are shown in Fig. 2d. The best device with PEDOT showed a PCE of 14.31% (13.35%), a J_{sc} of 21.18 mA cm^{-2} (21.13 mA cm^{-2}), a V_{oc} of 0.915 V (0.913 V) and a FF of 0.738 (0.691) for reverse and forward scanning. When PEDOT is replaced by a B-HTL, improved performance of the device is achieved with a J_{sc}, V_{oc}, FF, and PCE of 22.15 mA cm^{-2} (22.14 mA cm^{-2}), 1.015 V (1.014 V), 0.748 (0.736), and 16.85% (16.55%) for reverse and forward scanning, respectively. Here the superiority of the B-HTL is mainly embodied in the higher V_{oc} and J_{sc} of related PSCs. The external quantum efficiency (EQE) spectra and integrated current densities of the devices with PEDOT and B-HTL are shown in Fig. 2e and the latter has a higher spectral response in the whole spectrum.

Actually, considering that there are almost no differences in the absorption and film crystalline properties of the perovskite layers on two types of HTLs, the improved performance of the PSCs with the B-HTL should be attributed to the interfacial and the charge transporting behaviors. To confirm our assumption, Mott–Schottky analysis, steady photoluminescence (PL), conductivity characteristics and electrochemical impedance spectroscopy (EIS) are utilized to further investigate the potential efforts of the B-HTL.

It is known that the W_F values of transport materials could affect the built-in potential of heterojunction solar cells, thereby influencing the open voltage of the device.[22] Here the built-in potential (V_{bi}) is calculated by fitting the intercept of the linear regime with the *x*-axis of the Mott–Schottky plot. As shown in Fig. 3a, the V_{bi} values of the PSCs based on the B-HTL and PEDOT are equal to 0.83 V and 0.99 V, respectively. The deep W_F of the B-HTL is in favor of the large V_{bi} of the PSC, which affects the improvement of the V_{oc} to some extent.

In addition to the modified band alignment effect, the conductivity of the HTL also impacted the device performance. In particular, XRD measurements did not show obvious characteristic peaks that could be assigned to VO_x, explaining that the room-temperature sol–gel VO_x are amorphous (Fig. S7, ESI†). To compare the conductivities of the B-HTL and PEDOT, ITO/HTL/Ag sandwich structures are designed and *I*–*V* curves are measured under illumination conditions (shown in Fig. 3b). Under the same bias-voltage, larger current occurred on the structure with the B-HTL, showing more excellent conductivity. Thus the utilization of the B-HTL has a positive impact on charge transport.

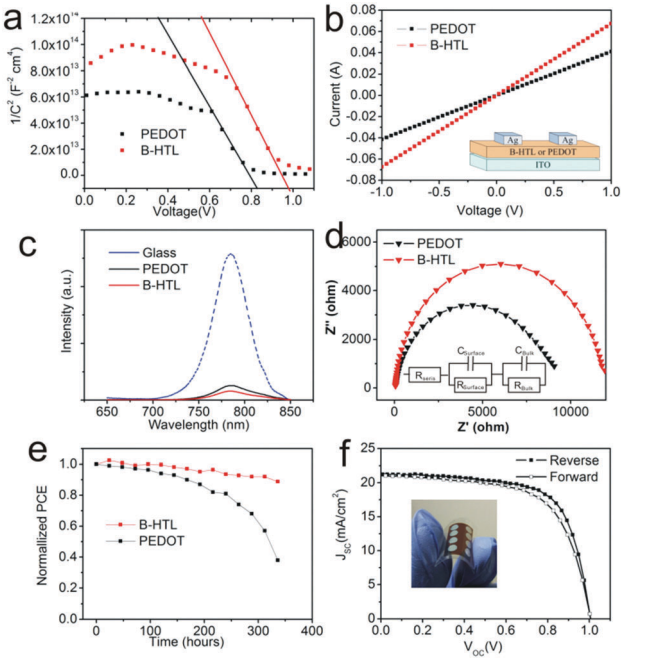

Fig. 3 (a) Mott–Schottky plots of PSCs with PEDOT and the B-HTL. (b) Conductivity measurements of different HTLs. (c) Steady PL spectra of perovskites on different substrates. (d) EIS and Nyquist models of PSCs based on different HTLs. (e) Normalised stability trends depicting the performances of the B-HTL and PEDOT devices under ambient conditions with no encapsulation (40% RH). (f) *J*–*V* curves of the flexible PSCs with a B-HTL.

The steady photoluminescence (PL) spectra of the perovskites on different substrates are also investigated. Fig. 3c shows a stronger PL intensity of the perovskite on the glass substrate at 782 nm, while the PL intensities of the perovskites on PEDOT and the B-HTL are significantly much lower, indicating that both PEDOT and the B-HTL can provide strong quenching channels for perovskite films, and the quenching effect induced by the B-HTL is more obvious. Here the effective charge carrier extraction should be attributed to both the excellent conductivity and favorable alignment of the B-HTL compared to PEDOT.

To investigate the interfacial charge transporting–recombination properties of the devices with different HTLs, electrochemical impedance spectroscopy (EIS) is carried out and the related results are shown in Fig. 3d. A simplified circuit model is given as the inset. The high-frequency and middle-frequency arcs are associated with the bulk (R_{bulk}) and surface (R_{sur}) recombination resistances of the device.[23] It is found that the R_{sur} of the PSC with the B-HTL is obviously larger than that of the PSC with PEDOT. Considering that the modification approach of the devices only affects the HTL, the decreased charge carrier recombination of the device with the B-HTL originated from the interface dynamic process, that is, the increase of the charge extraction at the HTL/perovskite interface and suppression of the interfacial recombination rate of the devices.

As shown in Fig. 3e, the stabilities of PSCs with a B-HTL and PEDOT were also studied. After 15 days, the PCE of the B-HTL employed PSC remained at about 10% of its original

performance, while the PCE of the device based on PEDOT degraded rapidly, maintaining only 40% of the initial efficiency. In fact, acidic and hygroscopic PEDOT would lead to corrosion of both the ITO and the perovskite film, causing the degradation of the device and the decomposition of the perovskite absorber layer. As comparison, the main body of the B-HTL is inorganic and stable VO_x material, which has good corrosion resistance.

Meanwhile, the following CuPc layer could serve as a hydrophobic "cover", further deterring the moisture attack. As shown in Fig. S8 (ESI†), a rather large contact angle of the B-HTL is measured as 84°, while the contact angle of the PEDOT film is only 41°. Such a stable and hydrophobic B-HTL could resist the invasion of moisture more effectively compared with the hydrophilic polymer HTL.

Benefiting from the low-temperature fabrication processes of the whole device, we prepared flexible PSCs based on a PET-ITO substrate. Correspondingly, the best performance with a PCE of 14.39%, a V_{oc} of 1.002 V, a J_{sc} of 21.21 mA cm^{-2} and a FF of 68% is obtained under reverse scanning (Fig. 3f). The slight PCE decrease and hysteresis of the flexible device compared to that of the rigid device may be due to the large series resistance and the weaker light transmittance of the PET-ITO substrate. The successful flexible application shows the advantage of the low-temperature processes. Actually, the highest temperature requirement of the fabrication is only 60 °C, which is under the glass transition temperature (T_g) of most polymers used as the matrices of the flexible electrodes, such as PET, PEN, PS and PC.[24,25]

In summary, a facile VO_x/CuPc B-HTL is developed and applied in planar heterojunction solar cells. This typical B-HTL contributes to the appropriate energy level matching at the HTL/perovskite interface and excellent conductivity, consequently improving the performance of PSCs by nearly 20%, compared with PEDOT. Meanwhile, remarkably increased stability of the device is achieved. At last, a flexible device with a B-HTL is also prepared because of its low-temperature and simplified fabrication process. On account of the experimental results and characteristic analysis, the typical bilayer HTL exhibits remarkable compatibility of perovskite solar cells in flexible and business fields.

This work was financially supported by the National Natural Science Foundation of China (Grant No. 11574248, 61604121, 61505161), the National Key R&D Program of China (Grant No. 2016YFB0400702), the China Postdoctoral Science Foundation (Grant No. 2016M590947), the Scientific Research Plan Projects of Shaanxi Education Department (Grant No. 17JK0700), the Natural Science Basic Research Plan of Shaanxi Province (Grant No. 2017JM6064), and the Fundamental Research Funds for the Central Universities (Grant No. xjj2016031). The SEM work was performed at the International Center for Dielectric Research (ICDR), Xi'an Jiaotong University, Xi'an, China. The authors thank Miss Dai for her help with using SEM. We also thank Dr Liu at the Instrument Analysis Center of Xi'an Jiaotong University for the assistance with UPS analysis.

Conflicts of interest

There are no conflicts to declare.

Notes and references

1 T. Leijtens, J. Lim, J. Teuscher, T. Park and H. J. Snaith, *Adv. Mater.*, 2013, **25**, 3227–3233.
2 A. Kojima, K. Teshima, Y. Shirai and T. Miyasaka, *J. Am. Chem. Soc.*, 2009, **131**, 6050–6051.
3 W. S. Yang, B. W. Park, E. H. Jung, N. J. Jeon, Y. C. Kim, D. U. Lee, S. S. Shin, J. Seo, E. K. Kim, J. H. Noh and S. I. Seok, *Science*, 2017, **356**, 1376–1379.
4 J. Xi, Z. X. Wu, K. Xi, H. Dong, B. Xia, T. Lei, F. Yuan, W. Wu, B. Jiao and X. Hou, *Nano Energy*, 2016, **26**, 438–445.
5 Z. L. Zhu, Y. Bai, T. Zhang, Z. K. Liu, X. Long, Z. H. Wei, Z. L. Wang, L. X. Zhang, J. N. Wang, F. Yan and S. H. Yang, *Angew. Chem., Int. Ed.*, 2014, **53**, 12571–12575.
6 L. Y. Yang, F. L. Cai, Y. Yan, J. H. Li, D. Liu, A. J. Pearson and T. Wang, *Adv. Funct. Mater.*, 2017, **27**, 1702613.
7 W. B. Yan, S. Y. Ye, Y. L. Li, W. H. Sun, H. X. Rao, Z. W. Liu, Z. Q. Bian and C. Huang, *Adv. Energy Mater.*, 2016, **6**, 1600474.
8 Y. D. Lin, B. Y. Ke, K. M. Lee, S. H. Chang, K. H. Wang, S. H. Huang, C. G. Wu, P. T. Chou, S. Jhulki, J. N. Moorthy, Y. J. Chang, K. L. Liau, H. C. Chung, C. Y. Liu, S. S. Sun and T. J. Chow, *ChemSusChem*, 2016, **9**, 274–279.
9 M. Li, Z. K. Wang, Y. G. Yang, Y. Hu, S. L. Feng, J. M. Wang, X. Y. Gao and L. S. Liao, *Adv. Energy Mater.*, 2016, **6**, 1601156.
10 Z. K. Wang, X. Gong, M. Li, Y. Hu, J. M. Wang, H. Ma and L. S. Liao, *ACS Nano*, 2016, **10**, 5479–5489.
11 Y. H. Lou, M. Li and Z. K. Wang, *Appl. Phys. Lett.*, 2016, **108**, 053301.
12 F. Igbari, M. Li, Y. Hu, Z. K. Wang and L. S. Liao, *J. Mater. Chem. A*, 2016, **4**, 1326–1335.
13 J. M. Wang, Z. K. Wang, M. Li, K. H. Hu, Y. G. Yang, Y. Hu, X. Y. Gao and L. S. Liao, *ACS Appl. Mater. Interfaces*, 2017, **9**, 13240–13246.
14 H. Zhang, J. Q. Cheng, F. Lin, H. X. He, J. Mao, K. S. Wong, A. K. Y. Jen and W. C. H. Choy, *ACS Nano*, 2016, **10**, 1503–1511.
15 H. C. Sun, X. M. Hou, Q. L. Wei, H. W. Liu, K. C. Yang, W. Wang, Q. Y. An and Y. G. Rong, *Chem. Commun.*, 2016, **52**, 8099–8102.
16 G. Yang, Y. L. Wang, J. J. Xu, H. W. Lei, C. Chen, H. Q. Shan, X. Y. Liu, Z. X. Xu and G. J. Fang, *Nano Energy*, 2017, **31**, 322–330.
17 J. M. Wang, Z. K. Wang, M. Li, C. C. Zhang, L. L. Jiang, K. H. Hu, Q. Q. Ye and L. S. Liao, *Adv. Energy Mater.*, 2018, **8**, 1701688.
18 W. J. Ke, D. W. Zhao, C. R. Grice, A. J. Cimaroli, G. J. Fang and Y. F. Yan, *J. Mater. Chem. A*, 2015, **3**, 23888–23894.
19 X. Q. Jiang, Z. Yu, H. B. Li, Y. W. Zhao, J. S. Qu, J. B. Lai, W. Y. Ma, D. P. Wang, X. C. Yang and L. C. Sun, *J. Mater. Chem. A*, 2017, **5**, 17862–17866.
20 X. Q. Jiang, Z. Yu, J. B. Lai, Y. C. Zhang, M. W. Hu, N. Lei, D. P. Wang, X. C. Yang and L. C. Sun, *ChemSusChem*, 2017, **10**, 1838–1845.
21 B. Xia, Z. X. Wu, H. Dong, J. Xi, W. Wu, T. Lei, K. Xi, F. Yuan, B. Jiao, L. X. Xiao, Q. H. Gong and X. Hou, *J. Mater. Chem. A*, 2016, **4**, 6295–6303.
22 C. Y. Liu, D. Z. Zhang, Z. Q. Li, X. Y. Zhang, W. B. Guo, L. Zhang, L. Shen, S. P. Ruan and Y. B. Long, *ACS Appl. Mater. Interfaces*, 2017, **9**, 8830–8837.
23 H. Dong, Z. X. Wu, J. Xi, X. B. Xu, L. J. Zuo, T. Lei, X. G. Zhao, L. J. Zhang, X. Hou and A. K. Y. Jen, *Adv. Funct. Mater.*, 2018, **28**, 1704836.
24 H. Dong, Z. X. Wu, Y. Q. Jiang, W. H. Liu, X. Li, B. Jiao, W. Abbas and X. Hou, *ACS Appl. Mater. Interfaces*, 2016, **8**, 31212–31221.
25 Y. Q. Jiang, J. Xi, Z. X. Wu, H. Dong, Z. X. Zhao, B. Jiao and X. Hou, *Langmuir*, 2015, **31**, 4950–4957.

